Optics Letters

Axial super-resolution evanescent wave tomography

Sarang Pendharker,[1] Swapnali Shende,[2] Ward Newman,[1,3] Stephen Ogg,[4] Neda Nazemifard,[2] and Zubin Jacob[1,3,*]

[1]Department of Electrical and Computer Engineering, University of Alberta, Edmonton, Alberta T6G 1H9, Canada
[2]Department of Chemical and Materials Engineering, University of Alberta, Edmonton, Alberta T6G 1H9, Canada
[3]Birck Nanotechnology Center, School of Electrical and Computer Engineering, Purdue University, West Lafayette, Indiana 47906, USA
[4]Department of Medical Microbiology & Immunology, University of Alberta, Edmonton, Alberta T6G 2E1, Canada
*Corresponding author: zjacob@purdue.edu

Received 4 October 2016; revised 3 November 2016; accepted 3 November 2016; posted 4 November 2016 (Doc. ID 276410); published 22 November 2016

Optical tomographic reconstruction of a three-dimensional (3D) nanoscale specimen is hindered by the axial diffraction limit, which is 2–3 times worse than the focal plane resolution. We propose and experimentally demonstrate an axial super-resolution evanescent wave tomography method that enables the use of regular evanescent wave microscopes like the total internal reflection fluorescence microscope beyond surface imaging and achieve a tomographic reconstruction with axial super-resolution. Our proposed method based on Fourier reconstruction achieves axial super-resolution by extracting information from multiple sets of 3D fluorescence images when the sample is illuminated by an evanescent wave. We propose a procedure to extract super-resolution features from the incremental penetration of an evanescent wave and support our theory by one-dimensional (along the optical axis) and 3D simulations. We validate our claims by experimentally demonstrating tomographic reconstruction of microtubules in HeLa cells with an axial resolution of ∼130 nm. Our method does not require any additional optical components or sample preparation. The proposed method can be combined with focal plane super-resolution techniques like stochastic optical reconstruction microscopy and can also be adapted for THz and microwave near-field tomography.

OCIS codes: (100.6640) Superresolution; (180.2520) Fluorescence microscopy; (180.6900) Three-dimensional microscopy; (100.6950) Tomographic image processing.

https://doi.org/10.1364/OL.41.005499

Optical tomography is a major tool in three-dimensional (3D) visualization of sub-micrometer-scale specimens in biology, material sciences, and nano-fabrication technology [1–3]. Tomographic reconstruction is done by optical sectioning the object in the focal plane, followed by 3D stitching of the acquired z-stack of focal plane images. The resolution of a 3D tomographic reconstruction of an object is therefore governed by the focal plane resolution and the axial resolution of the underlying optical image acquisition. A wide range of well-advanced fluorescence-based super-resolution microscopy techniques have been reported and are currently in practice [4]. Super-resolution in the focal plane can be achieved by localization techniques like stimulated emission depletion (STED) [5], stochastic optical reconstruction microscopy (STORM) [6], and photo-activated localization microscopy [7], or by patterned illumination techniques like structured illumination microscopy [8], plasmonic structured illumination microscopy (PSIM) [9], etc. Even though many focal-plane super-resolution techniques are available, accurate 3D tomographic reconstruction still remains a challenge due to the ellipsoidal shape of the point-spread function (PSF), which makes resolution in the axial direction 2–3 times worse [10]. The 4Pi [11] and I^5M microscopes [12] have increased the resolution in the axial direction with an almost spherical PSF. More recently, a triple-view capture and fusion approach [13] has been reported to improve volumetric resolution by a factor of two. However, these techniques require imaging and illuminating the same focal plane from both sides of the sample and depend on extensive optical components and precise optical phase matching. 3D STED [1] and 3D STORM [2,3] for 3D localization have also been reported. Axial super-resolution can also be achieved by placing a reflective mirror behind the sample to squeeze the PSF in the axial direction by interference from the reflected STED beam [14,15]. However, STORM and STED impose constraints on the properties of the fluorescent probes, limiting their applicability to imaging photo-switchable fluorophores and samples with a sharp emission spectrum, respectively. Evanescent wave illumination techniques like total internal reflection fluorescence (TIRF) microscopy [16,17], plasmon-enhanced TIRF [18], variable-angle TIRF [19], and pseudo-TIRF [20] provide super-resolution along the optical axis with very high signal-to-noise ratios (SNRs) without imposing constraints on the fluorescence properties of the sample. However, the capabilities of the evanescent wave techniques are so far

limited to near-surface imaging, thus making them unfit for direct 3D tomography. Three-dimensional geometric estimation from a large number of TIRF surface images captured at different incident angles has been recently reported [21,22]. These methods require solving inverse estimation problems and prior knowledge of the sample features. More recently, a simpler protocol of sequential imaging and photobleaching with multi-angle TIRF to localize the fluorescence emission to a region within the PSF of the objective was reported to achieve axial super-resolution [23].

In this Letter, we propose an axial super-resolution evanescent wave tomography (AxSET) method based on TIRF microscopy. We extract features with super-resolution from multiple sets of diffraction-limited 3D images, where each set of 3D images is acquired at different illumination depths of the TIR evanescent wave. The proposed method does not require explicit knowledge of the illumination depth or the PSF, nor does it rely on photobleaching the sample. The method is tolerant to local variations in the refractive index of the sample and the angular bandwidth of the incident beam. We present the theoretical basis of our algorithm and show that it enables 3D tomography without additional optical components and sample preparation. We support our claims with one-dimensional (1D) and 3D Fourier optics simulations and show that our algorithm can discern and reconstruct objects that otherwise appear coalesced with a conventional microscope. We experimentally validate our method by imaging and demonstrating super-resolution reconstruction of microtubules in HeLa cells. We demonstrate tomographic reconstruction with an axial resolution of ~130 nm (in contrast to the >450 nm limit of the microscope). Although the main goal of this Letter is to increase the resolution in the axial direction, our method can be combined with other focal-plane super-resolution techniques like STORM and PSIM to achieve 3D super-resolution.

The resolution limit arising from the ellipsoidal shape of the PSF of an optical microscope is $\Delta r \approx \lambda/(2n \sin \phi)$ in the focal plane and $\Delta z \approx \lambda/(n \sin^2 \phi)$ along the optical axis [10]. Here, λ is the wavelength of light in free space, n is the refractive index of the medium, and ϕ is the aperture angle of the lens. The axial resolution, which is worse by a factor greater than two as compared to the focal-plane resolution, is significantly enhanced if, instead of a propagating wave, the fluorescence in the sample is excited by an evanescent wave generated by the TIR at the interface of cover slip and the sample, as shown in Fig. 1. The attenuation coefficient of an evanescent wave in the sample is given by $\alpha = (2\pi/\lambda)(n_1^2 \sin^2\theta - n_2^2)^{(1/2)}$, where n_1 is the refractive index of the cover slip, and n_2 is the refractive index of the sample. θ is the angle between the incident light and the normal to the interface. When the incident angle of light (θ) is above the critical angle $\theta_c = \sin^{-1}(n_2/n_1)$, the wave is evanescent in the sample, with a theoretical upper limit to the attenuation being $\alpha_{\max} = (2\pi/\lambda)(n_1^2 - n_2^2)^{(1/2)}$. Since the attenuation α of the wave can be controlled between 0 and $\alpha_{\max}$ by the incident angle θ, it is possible to allow illumination of a desired thickness and acquire a z-stack of the focal plane images over the desired thickness, as depicted in Fig. 1. The 3D image thus obtained will have a high SNR, but since the image is captured via a conventional optical microscope, the resolution of each focal plane image will be diffraction limited and will be governed by an ellipsoidal PSF. Thus, tomography with optical sectioning is diffraction limited in the axial direction,

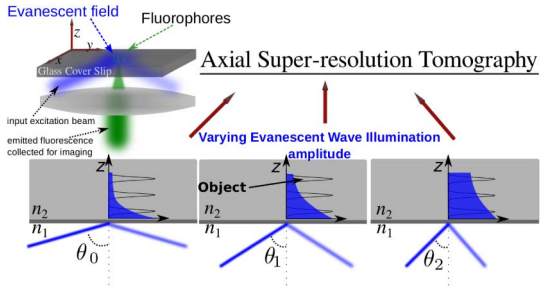

Fig. 1. Schematic of a TIRF microscope. The penetration depth of an evanescent wave can be controlled by the incident angle θ of the illuminating beam. As the incident angle is increased, the illumination depth decreases. When illumination depth of the sample increments in discrete steps, the information captured within the PSF of the objective lens also increments in steps, and the incremental information corresponds to super-resolution features.

even in the evanescent wave illumination mode. However, due to evanescent wave illumination, near-surface features have higher amplitudes than those at deeper planes, and this is reflected in the Fourier components of the corresponding features in the acquired images. By comparing the Fourier components of two images with different illumination depths, features at deeper planes can be identified at a resolution greater than the diffraction limit. In other words, axial super-resolution features can be extracted from the diffraction-limited images by eliminating the near-surface super-resolution features captured in high-resolution TIRF illumination mode. We call this method AxSET.

The concept of AxSET is explained in Fig. 2. Figure 2(a) shows the spatial distribution ($f_{\text{object}}(z)$) of the sample in the z direction, and its Fourier representation ($F_{\text{obj}}(k_z)$) is shown in the inset. For illustration, we have considered a two-particle object. Both the particles in the object as well as the separation between them leave their signature throughout the Fourier domain. Since the optical transfer function of the microscope is band limited, the Fourier representation of the image obtained by conventional imaging is truncated, and the two particles appear coalesced in the spatial domain if they are closer than the resolution limit [black dashed curve in Fig. 2(b)]. This image is therefore diffraction limited. Figure 2(c) depicts the image acquired from the same object f_{obj} in the TIRF mode. Before the image is acquired by the optical microscope, the object is illuminated by an evanescent wave $f_{\text{ev}} = e^{-\alpha z}$, resulting in the differential amplitude of the particles at different depths, such that only the particle near the surface ($z = 0$ plane) is prominent. Therefore, the Fourier representation of the TIRF illuminated object has a signature of only the first particle. Note that the object and evanescent wave illumination multiply in the spatial domain and convolve in the Fourier domain. When this differentially illuminated object is imaged by the optical microscope, the resultant truncation of the Fourier spectrum (F_{TIRF}) leads to the elongation of the reconstructed particle (f_{TIRF}), but nevertheless, the particle can be distinctly identified at its correct position. This image, represented by f_{TIRF}, is therefore super-resolved near the surface. The difference between the conventional and TIRF images is that even in the band-limited Fourier representation, the conventional image has signatures from both particles, while in the

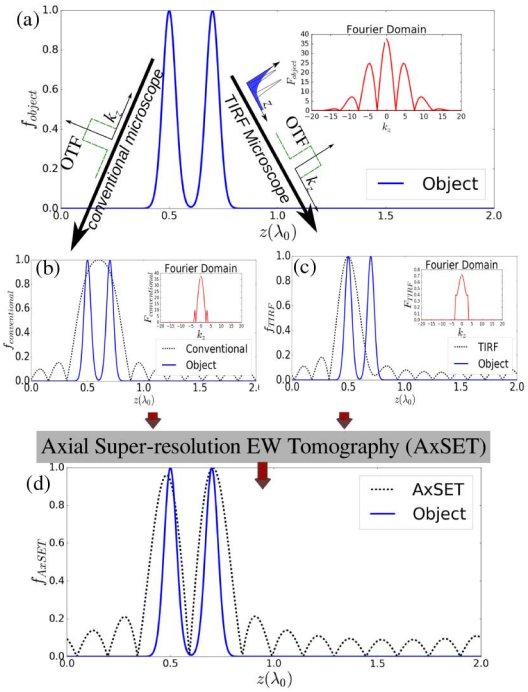

Fig. 2. Fourier reconstruction with confocal and TIRF images. f_{obj} and F_{obj} are the object in the spatial domain and Fourier domain, respectively. In conventional microscopy the object is passed through the optical transfer function. The band-limited optical transfer function of the microscope introduces the diffraction limit, and the resultant captured image $f_{\text{conventional}}$ is diffraction limited, as shown by the blue curves in left panel. The same object when imaged by the TIRF is first illuminated with an evanescent wave, and the differentially illuminated object is then imaged by a conventional system to get super-resolution f_{TIRF}. A Fourier reconstruction is then performed on $F_{\text{conventional}}$ and F_{TIRF} to extract and reconstruct the object with super-resolution.

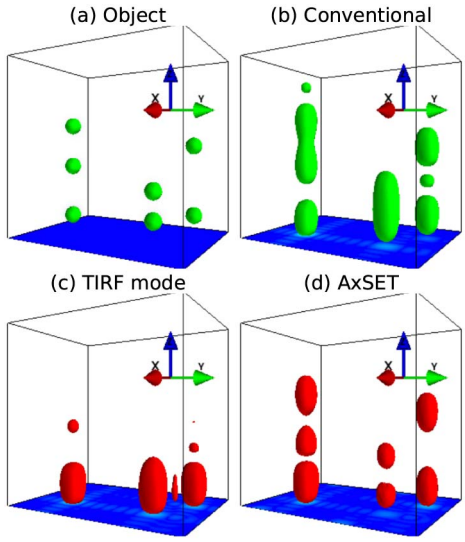

Fig. 3. AxSET reconstruction of a multi-particle 3D object. Panel (a) shows the digitally created object. (b) shows the 3D image of the object formed by the conventional imaging. (c) shows the 3D image formed in the TIRF surface mode, and (d) shows the super-resolution AxSET image formed by processing the images in (b) and (c).

TIRF, the signature of the particle from the deeper layers is lost. We will call the signature that is lost in the TIRF but present in conventional fluorescence microscopy $F_{\text{residue}}(k_z)$. The expression relating the TIRF and conventional images can then be written as

$$F_{\text{conventional}}(k_z) = C * F_{\text{TIRF}}(k_z) + F_{\text{residue}}(k_z). \quad \textbf{(1)}$$

C is a scaling factor, which in general can be a function of k_z. We solve Eq. (1) using a deconvolution operation between $F_{\text{conventional}}$ and F_{TIRF} and compute the F_{residue}. F_{residue} has super-resolution information, which, when combined with F_{TIRF}, gives the AxSET reconstructed object as

$$F_{\text{AxSET}}(k_z) = F_{\text{TIRF}}(k_z) + F_{\text{residue}}(k_z). \quad \textbf{(2)}$$

The reconstructed object is represented by a black dashed line in Fig. 2(d), and the original object is shown by the blue curve. It can be seen that while a conventional microscope shows the two objects as coalesced and TIRF shows only the near-surface object, the AxSET reconstructed image distinctly shows both the objects. Note that the Fourier representation is in complex space, where the phase of the signal has critical information. Equation (2) is therefore not equivalent to the simple addition of the amplitudes. When there are multiple objects, we might need to extract the features sequentially for incrementally increasing penetration. The axial resolution limit of the proposed method is limited by the ability of the attenuating illumination to discern features between two adjacent layers of the sample. Therefore, the achievable axial resolution will be higher near the surface and would approach the diffraction limit for deeper illumination.

Next, we implement AxSET to perform 3D tomography of a digitally created multi-particle object, as shown in panel (a) of Fig. 3. The 3D image of the object from a conventional microscope when the full depth of the object is illuminated is shown in panel (b). It can be seen that in the 3D image, the individual particles, which are all spheres, appear elongated and some particles are coalesced. The same object, when imaged in the surface illumination mode, gives the 3D reconstruction as shown in panel (c). In the surface illumination mode, only the particles close to the surface ($z = 0$ plane) are visible. For reconstruction, the actual distribution of the object is unknown. All we have are the images in Figs. 3(b) and 3(c). When the 3D images in Figs. 3(b) and 3(c) are processed as per Eqs. (1) and (2), we get the 3D AxSET reconstruction as shown in Fig. 3(d). The reconstructed tomography matches well with the original distribution of particles in the object. It should be noted that the proposed AxSET method simultaneously generates high-fidelity tomographic reconstructions of particles that are closer than the diffraction limit, as well as those that are scattered further away. Thus, our method is suitable for super-resolution tomographic reconstruction of samples with a variety of features along the axial direction. It can be seen that the lower left particle in the AxSET reconstructed image is more elongated as compared to the other reconstructed particles. This is because along the line of three particles, the AxSET reconstruction with two of the image sets extracts super-resolution features of only the deeper-plane particles. Better resolution can be achieved with more sets of 3D images.

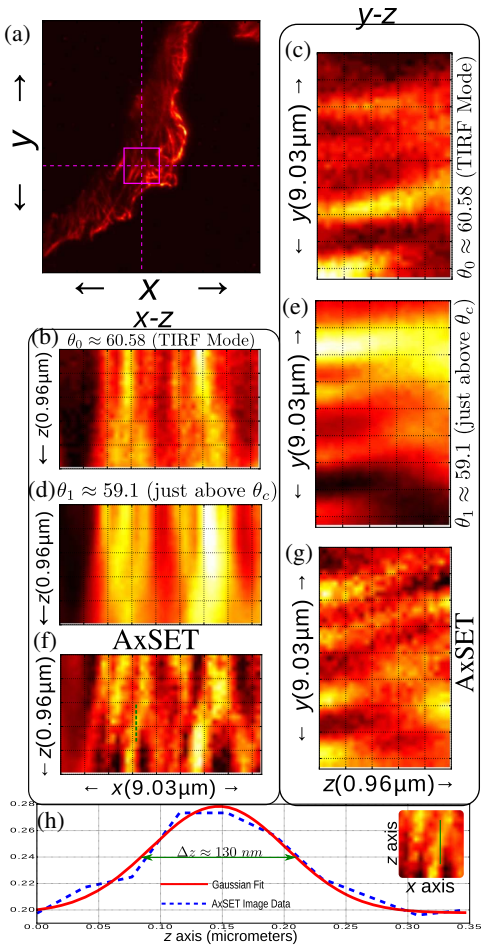

Fig. 4. AxSET reconstruction of microtubule structures in HeLa cells stained with alexafluor 488. Panel (a) shows an x–y plane optical section of the sample, and the region of interest (ROI) is shown by the solid magenta square. (b) and (c) show the TIRF mode in the x–z and y–z planes of the ROI at cross-wires [dashed magenta lines in (a)], respectively. (d) and (e) show the corresponding x–z and y–z planes in the conventional illumination mode. The TIRF and conventional 3D images are processed by AxSET, and the planes of reconstructed super-resolution image are shown in (f) and (g). (h) shows axial data of a microtubule with a resolution of about 130 nm.

We validate our method on microtubule structures in HeLa cells tagged with alexafluor 488 fixed on a glass cover slip ($n_1 = 1.55$). The cells are immersed in an aqueous medium ($n_2 = 1.33$). Figure 4(a) shows the x–y plane optical section of the sample. The imaging was performed on a Nikon Eclipse Ti TIRF microscope with a 100x objective and a 1.49 numerical aperture. The sample is imaged at two illumination angles, $\theta_0 \approx 60.58°$ for surface illumination and $\theta_1 \approx 59.1°$ (close to the critical angle) for deeper illumination. The x–z and y–z plane axial sections of the 3D image at θ_0 illumination are shown in Figs. 4(b) and 4(c), respectively, while Figs. 4(d) and 4(e) show the corresponding x–z and y–z plane axial sections for θ_1 illumination, respectively. Processing these 3D images with the proposed AxSET method yields the super-resolution image whose axial sections are shown in Figs. 4(f) and 4(g). It can be seen that the features that were blurred and smeared out in the raw images can be seen with a precision of around 130 nm in the reconstructed image. Figure 4(h) shows the cut-through of the AxSET image along one microtubule. The resolution of the microscope is 210 nm in the focal plane and ~450 nm along the optical axis. The processed image clearly shows resolution enhancement by a factor of ~3 along the z-axis.

The proposed AxSET enables full 3D tomographic reconstruction with axial resolutions higher than the optical acquisition system allows. This method can be employed to extract super-resolution features wherever an evanescent wave can be used to excite the sample. This method can be combined with focal plane super-resolution techniques like STORM and will find applications in wide range of 3D microscopy techniques ranging from optical to THz imaging.

Funding. Institute for Oil-Sands Innovation (IOSI), Canada.

Acknowledgment. The authors thank Gareth Lambkin from Biological Services, Department of Chemistry, University of Alberta, for the technical support.

REFERENCES

1. C. Osseforth, J. R. Moffitt, L. Schermelleh, and J. Michaelis, Opt. Express **22**, 7028 (2014).
2. B. Huang, W. Wang, M. Bates, and X. Zhuang, Science **319**, 810 (2008).
3. K. Xu, H. P. Babcock, and X. Zhuang, Nat. Methods **9**, 185 (2012).
4. B. Huang, H. Babcock, and X. Zhuang, Cell **143**, 1047 (2010).
5. S. W. Hell and J. Wichmann, Opt. Lett. **19**, 780 (1994).
6. R. E. Thompson, D. R. Larson, and W. W. Webb, Biophys. J. **82**, 2775 (2002).
7. G. Patterson, M. Davidson, S. Manley, and J. Lippincott-Schwartz, Annu. Rev. Phys. Chem. **61**, 345 (2010).
8. M. G. Gustafsson, J. Microsc. **198**, 82 (2000).
9. F. Wei, D. Lu, H. Shen, W. Wan, J. L. Ponsetto, E. Huang, and Z. Liu, Nano Lett. **14**, 4634 (2014).
10. S. W. Hell, Science **316**, 1153 (2007).
11. S. Hell and E. H. Stelzer, J. Opt. Soc. Am. A **9**, 2159 (1992).
12. M. Gustafsson, D. Agard, and J. Sedat, J. Microsc. **195**, 10 (1999).
13. Y. Wu, P. Chandris, P. W. Winter, E. Y. Kim, V. Jaumouillé, A. Kumar, M. Guo, J. M. Leung, C. Smith, I. Rey-Suarez, H. Liu, C. M. Waterman, K. S. Ramamurthi, P. J. L. Riviere, and H. Shroff, Optica **3**, 897 (2016).
14. T. Deguchi, S. Koho, T. Näreoja, and P. Hänninen, Opt. Rev. **21**, 389 (2014).
15. X. Yang, H. Xie, E. Alonas, Y. Liu, X. Chen, P. J. Santangelo, Q. Ren, P. Xi, and D. Jin, Light Sci. Appl. **5**, e16134 (2016).
16. D. Axelrod, Methods Cell Biol. **89**, 169 (2008).
17. H. Shen, E. Huang, T. Das, H. Xu, M. Ellisman, and Z. Liu, Opt. Express **22**, 10728 (2014).
18. K. Balaa, E. Fort, and N. Instruments, Imaging Microsc. **11**, 55 (2009).
19. Y. Wan, W. M. Ash, L. Fan, H. Hao, M. K. Kim, and J. Lin, Plant Methods **7**, 1 (2011).
20. W. Sun, A. Xu, K. Marchuk, G. Wang, and N. Fang, J. Assoc. Lab. Autom. **16**, 255 (2011).
21. Q. Yang, A. Karpikov, D. Toomre, and J. Duncan, in *International Conference on Medical Image Computing and Computer-Assisted Intervention* (2010), 538.
22. J. Boulanger, C. Gueudry, D. Münch, B. Cinquin, P. Paul-Gilloteaux, S. Bardin, C. Guérin, F. Senger, L. Blanchoin, and J. Salamero, Proc. Natl. Acad. Sci. USA **111**, 17164 (2014).
23. Y. Fu, P. W. Winter, R. Rojas, V. Wang, M. McAuliffe, and G. H. Patterson, Proc. Natl. Acad. Sci. USA **113**, 4368 (2016).